R. Ryan Vallance*
e-mail: vallance@gwu.edu
Precision Systems Laboratory,
The George Washington University,
738 Phillips Hall,
801 22nd St., N.W., Washington, DC 20052

Eric R. Marsh
Machine Dynamics Research Laboratory,
The Pennsylvania State University,
21 Reber Building,
University Park, PA 16802

Philip T. Smith
Mechanical Engineering,
University of Kentucky,
015 Ralph G. Anderson Building,
Lexington, KY 40506

Effects of Spherical Targets on Capacitive Displacement Measurements

Capacitive displacement sensors are widely used in precision manufacturing and metrology because they measure displacements with nanometer resolution. Prior literature usually treats capacitive sensors consisting of electrodes arranged as parallel plates. In this work, the target electrode is spherical, which is common in machine tool metrology, spindle metrology, and the measurement of sphericity. The capacitance due to a gap between flat and spherical electrodes is less than that of two flat electrodes, which causes four effects. As the diameter of the target electrode is reduced, the sensitivity increases, the sensing range decreases, the sensing range shifts toward the target, and the sensor becomes nonlinear. This paper demonstrates and quantifies these effects for a representative capacitive sensor, using finite element analysis and experimental testing. For larger spheres, the effects are correctible with apparent sensitivities, but measurements with the smallest spheres become increasingly nonlinear and inaccurate.
[DOI: 10.1115/1.1813476]

1 Introduction

Capacitive displacement sensors are used in a variety of manufacturing applications that require noncontact measurements with microscale range and nanoscale resolution. Within the field of precision engineering, capacitive sensors are used to sense fine motion, measure positioning error (e.g., straightness, squareness, and ball bars), and inspect workpieces (e.g., roundness, cylindricity, sphericity). Capacitive sensors present a relatively inexpensive, robust, and easy-to-use solution to these and other measurement challenges.

A common realization of the capacitive sensor is a sensing electrode and guard ring enclosed within a grounded sensor body. Figure 1 shows this configuration of a commercial sensor used in precision applications. The sensor is positioned perpendicular to a target electrode formed by a conductive surface in a workpiece, machine, or instrument. In many instruments and in fine motion control, the target is usually a flat surface with characteristic dimensions significantly larger than the sensing electrode, which can be as small as one millimeter. However, other applications common in machine and workpiece metrology require target electrodes that are not flat. For example, ASME standards for evaluating machine tools [1,2] describe several tests to measure errors with capacitive sensors targeting spherical or cylindrical surfaces. Another example is the ultraprecision measurement of spindle error motion, which is usually made with capacitive sensors and lapped spherical artifacts [3,4].

It is standard practice for commercial capacitive sensors to be factory calibrated with flat target surfaces. This paper shows how measurements taken with sensors targeting spherical surfaces lead to four sources of error if the sensors are calibrated with flat targets. First, the sensitivity of the sensor increases resulting in exaggerated displacement measurements. Furthermore, the sensing range is both decreased and shifted toward the target. Finally, the otherwise linear output of the sensor system becomes increasingly nonlinear for targets of decreasing diameter.

To investigate the severity of these effects, a capacitive sensor (Fig. 1) is evaluated with spherical targets having diameters less than 25.4 mm. Complexities in this sensor preclude a simple analytical model so an approach using the finite element method is used. The results from the finite element analysis are validated experimentally by comparing the output of two capacitive sensors, one targeting a flat reference surface and another targeting a spherical surface. The excellent agreement of the finite element and experimental results suggest that either approach is valid for quantifying these effects. The output of the sensor with larger spheres is easily corrected with apparent sensitivities,[1] but the nonlinear effects with small spheres become so significant that accurate measurements are not achieved.

2 Background and Literature Review

Capacitive displacement sensors are constructed from conductive electrodes that operate under a potential difference when separated by a dielectric material. The sensor's electrodes are often flat surfaces [5–8], but cylindrical and spherical electrodes are also constructed [9,10]. As shown in Eq. (1), the theoretical (ideal) capacitance C between two flat and parallel electrodes separated by a small gap is proportional to the permittivity of free space ε_o, the relative permittivity of the dielectric material separating the sensor and target ε_r, and the area of the sensing electrode A; the capacitance is inversely proportional to the gap g that separates the sensor and target. The permittivity of free space is a constant equal to 8.854×10^{-12} F/m, and the relative permittivity is the ratio of the dielectric's permittivity to the permittivity of free space

$$C=\frac{\varepsilon_o\varepsilon_r A}{g} \tag{1}$$

Relative displacements between the electrodes alter the capacitance by changing either the distance between the plates or the overlapping area of the plates. Capacitive sensors that use changes in the gap are generally more sensitive, but suitable to small displacement ranges [6,7,11], while sensors that use changes in the area are less sensitive but suitable for larger displacement ranges [12–14]. For this reason, capacitive sensors used in precision applications, such as metrology, often observe changes in the gap. The hyperbolic relation between capacitance and gap is of little consequence since the inverse of capacitance C^{-1} is linearly proportional to g as shown in Eq. (2)

*Corresponding author.

Contributed by the Manufacturing Engineering Division for publication in the JOURNAL OF MANUFACTURING SCIENCE AND ENGINEERING. Manuscript received January 13, 2004; revised April 2, 2004. Associate Editor: T. R. Kurfess.

[1] The term *apparent sensitivity* is used throughout this paper to distinguish the sensitivity with a spherical target from the sensitivity determined by calibration with a flat target.

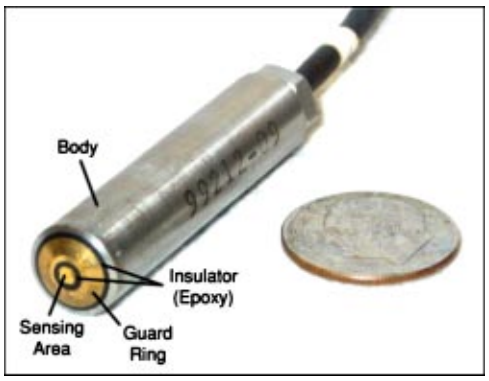

Fig. 1 Representative capacitive displacement sensor (Lion Precision C1-C)

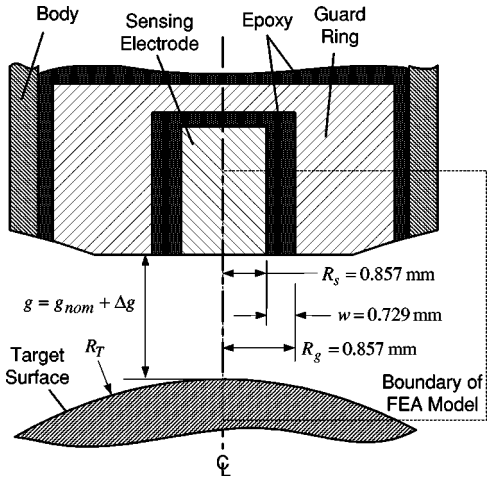

Fig. 2 Axisymmetric electrodes in representative sensor and spherical target

$$C^{-1} = \frac{g}{\varepsilon_o \varepsilon_r A} \tag{2}$$

Small changes in capacitance are often detected with AC bridges [15], such as the transformer ratio bridge [5,6,8,16,17] or a variety of other circuits [18–21]. The circuits compare the capacitance between the sensing electrodes to a reference capacitance that corresponds to a particular nominal gap g_{nom}. With further signal conditioning, an analog voltage V is produced so that V equals zero when g equals g_{nom}. This leads to the linear sensing relation in Eq. (3), where output V is proportional to changes in the gap Δg. The work presented in this paper is independent of the type circuit that produces this relation. For an ideal parallel plate capacitive sensor, the proportionality constant commonly called sensitivity S, depends on the gain of the electronics G, the permittivities, and the surface area of the sensing electrode as shown in Eq. (4). However, the sensitivity may be dramatically affected by other factors as described in this work

$$V = S\Delta g \tag{3}$$

$$S \approx \frac{G}{\varepsilon_o \varepsilon_r A} \tag{4}$$

Sensors for precision applications, such as the sensor in Fig. 1, generally use axisymmetric electrodes that target flat surfaces, similar to one described by Richards [22]. The sensor's face includes a cylindrical electrode (with circular sensing area) that is separated from an annular electrode known as the guard ring. The guard ring, originally suggested by Kelvin, improves the homogeneity of the electric field between the sensing electrode and target when the guard ring and sensing area are at the same potential. Maxwell [23] analyzed the effect of the guard ring and showed that the increase in capacitance due to the field fringing into the annulus between the guard ring and sensing area can be as small as a few parts per million if the radial separation w between the sensing electrode and guard ring is very small compared to the gap g. In such cases, the capacitance between the sensing electrode and target is reasonably predicted with Eq. (1).

The capacitance can also be analytically determined for a few other geometries and boundary conditions in three nontrivial steps: solve Laplace's equation for the potential distribution in the space between the electrodes, calculate the charge collected on the electrodes, and calculate the capacitance as the ratio of the charge and voltage difference. Using this approach, Heerens and Vermeulen [24] presented analytical solutions for the capacitance of sensors with modified edge geometries, and Heerens [25,26] later presented solutions for additional cylindrical and toroidal configurations.

In practice, the measured capacitance usually differs from the analytical predictions. This discrepancy is attributable to a variety of physical and electrical factors. Electrical factors may include stray capacitance [20], temperature drift [22], and dynamic hysteresis [27]. Hicks and Atherton [28] discuss several physical factors that are included in the following list:

- finite width of the annular guard ring [5,29]
- thermal expansion of electrodes [6]
- fringing of the electric field between the sensing electrode and guard ring [7,23,29,30]
- variation in the relative permittivity due to temperature and pressure fluctuations [22]
- nonflatness or noncoplanarity of the electrodes [28,29]
- nonparallelism (tilt) of the sensor's face and target surface [29,33,31,32],
- roughness or damage to the sensing electrode, guard ring, or target surfaces [33],
- thickness of the electrodes [33]
- elastic deformation due to electrostatic forces [34]

Complex geometries and boundary conditions in modern sensors can require that Laplace's equation be solved numerically with finite element analysis (FEA). Some researchers used FEA to predict how the capacitance between electrodes varies with displacement [35–38]. With FEA, the effects of nonideal physical factors, such as those listed above, can be included. For instance, Lányi [39] used FEA to investigate errors and nonlinearity resulting from manufacturing imperfections in the electrodes.

Capacitive displacement-sensing systems are calibrated to verify their actual sensitivity and to also measure their nonlinearity. This is accomplished by changing the gap between the sensor and a target surface while comparing the output voltage V to measurements made by an independent displacement-measuring interferometer or sensor [30], a traceable calibrated linear scale, or a Fabry-Perot etalon with a He-Ne laser [40]. Calibration of commercial sensors is typically done in air with sensors targeting a flat surface.

This paper quantifies the effects of using a capacitive sensor with a spherical target as illustrated in Fig. 2. The electronics with this sensor provide two sensing ranges, one with low sensitivity ($-0.394\ \text{V}/\mu\text{m}$) and another with high sensitivity ($-1.969\ \text{V}/\mu\text{m}$). The nominal gap and sensitivity determined by calibration in air and with a flat target are summarized in Table 1. The capacitance between the sensing electrode and a flat target cannot be predicted by Eq. (1) or other analytical solutions for at least three reasons. First, the annular distance between the sensing electrode and guard ring w is not much smaller than the nominal gap g_{nom}. Second, the sensor uses an epoxy insulator ($\varepsilon_r \approx 3.8$) between the sensing electrode and guard ring, which affects the

Table 1 Nominal gaps, sensitivities, and nonlinearities for low and high sensitivities of the representative capacitive sensor

	Sensing range (μm)	Nominal gap, g_{nom} (μm)	Sensitivity, S (V/μm)	Nonlinearity, %FS
Low sensitivity	76.2–127.0	101.6	−0.394	0.02
High sensitivity	20.3–30.5	25.4	−1.969	0.33

output of the sensor as described by Kahn [30]. Third, the guard ring is not entirely flat. These considerations preclude the use of analytical solutions for capacitance, but the performance of modern sensors is excellent. The calibration data show that the sensor is linear within 0.33% over the full measurement range when targeting a flat surface.

The effects of using a representative sensor with spherical targets are investigated with finite element analyses and experiments in the remainder of the paper. Section 3 describes a finite element analysis that yields capacitance and inverse capacitance as a function of target diameter and the gap distance. Section 4 uses the capacitance data to illustrate the effects of target diameter on sensitivity and sensing range. Section 5 presents experiments that validate the finite element analyses and further reveal that nonlinearity increases significantly for spherical targets with small diameters.

3 Capacitance as a Function of Gap and Target Diameter

The dimensions, geometry, and materials of a modern capacitive sensor may not measure a capacitance that agrees with analytical solutions. However, finite element analyses (FEA) can determine the capacitances even when sensors are constructed with multiple electrodes, complex geometry, complex boundary conditions, or multiple dielectric materials. This section, therefore, describes an FEA procedure for capacitive sensors; although the details of the geometry are sensor specific, the procedure is general. The results of the FEA procedure are the lumped capacitance between the sensing electrode and spherical target as a function of two variables, the gap and the target diameter.

3.1 Procedure for Finite Element Analyses. Capacitance values for many combinations of electrode gap and target diameter are necessary to reveal nonlinearities, so the analysis was conducted in ANSYS with a set of scripts that repeatedly execute the procedure in Fig. 3 [41]. The three-dimensional (3D) geometry of the cylindrical commercial sensor targeting a spherical electrode is reduced to two-dimensional (2D) axisymmetric geometry to significantly reduce the number of finite elements and calculation time. The axis of symmetry coincides with the centerline of the sensor and the center of the spherical target. This analysis primarily uses a 2D quadrilateral element for axisymmetric electrostatic problems (Type 121). Special quadrilateral elements are used at the perimeter of the geometry to accurately model infinite boundary conditions (Type 110). Both types of elements have one degree of freedom at their nodes that is used to calculate the potential distribution within the two dielectric materials. The epoxy that separates the sensing electrode and guard ring has a relative permittivity of 3.8, and the air between the sensor and target has a relative permittivity of 1.0008.

The modeled geometry, which is enclosed by a dashed rectangle in Fig. 2, includes the sensing electrode, guard ring, body, target, epoxy insulators, and the air between the sensor and target. Only the areas for the dielectric material (epoxy and air) are meshed because there is no change in potential within the conductive electrodes. The density of the mesh was evaluated and adjusted to achieve reliable convergence with acceptable solution time. The density of the mesh is highly concentrated in the regions near the sensing element, with relatively large elements at the perimeter of the axisymmetric geometry.

Two exemplary results from an electrostatic finite element analysis are shown in Figs. 4 and 5. Figure 4 shows a contour plot of the electric potential within the dielectric epoxy and air when a fixed potential (9 V) is applied to the sensing area and guard ring while the housing and target are grounded (0 V). It is important to observe the potential gradients in the air gap between the sensing electrode and target and also in the epoxy that separates the sensing electrode from the guard ring. These gradients indicate the fringing of the electric field beyond the sensing electrode. Figure 5 shows a quiver plot of the electric field in the vicinity of the electrodes. As expected, the field is not uniform in the region between the sensing electrode and the target; the field is strongest along the axis of symmetry and is lower at the perimeter of the sensing electrode. The direction of the gradient also changes due to the sharp edge geometry around the perimeter of the sensing area.

Although the distribution of electric potential and the electric field are of some interest, the capacitance between electrodes is more meaningful for assessing the effect of a spherical target. As shown in Fig. 6, the four electrodes in the sensor and target lead to

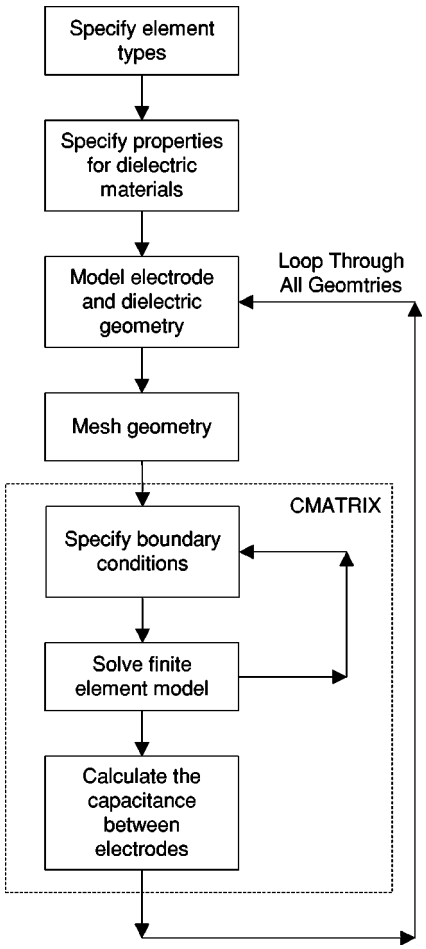

Fig. 3 Finite element analysis procedure

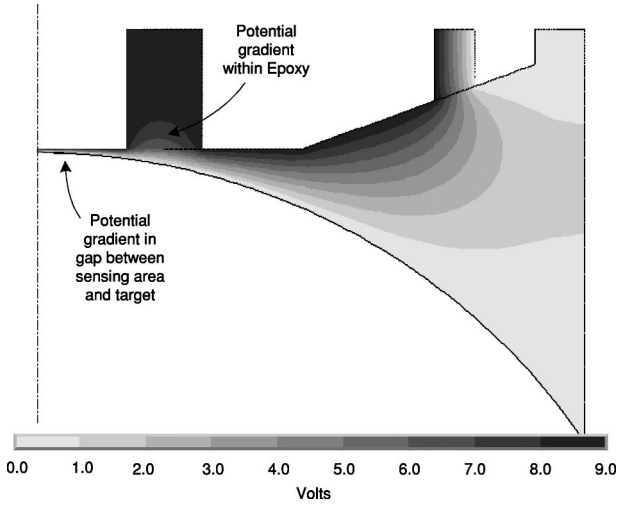

Fig. 4 Electric potential (0–9 V) within air gap and epoxy in vicinity of electrodes

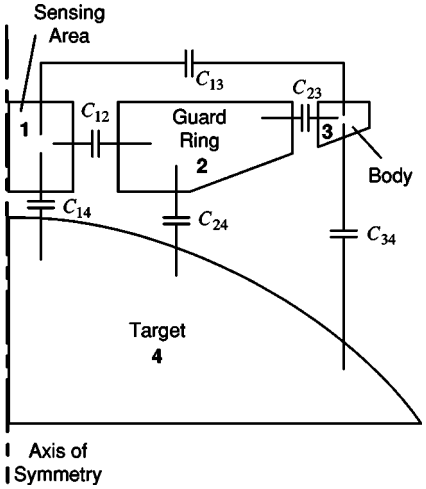

Fig. 6 Lumped capacitances between conductive electrodes

four mutual capacitances and six capacitances between electrodes. ANSYS provides the CMATRIX macro for determining the lumped capacitances in problems with multiple electrodes, and Smith [41] thoroughly demonstrated how this macro is used to determine the ten capacitances in the present problem. As illustrated in the FEA procedure of Fig. 3, the CMATRIX macro applies appropriate boundary conditions (fixed voltages) to the electrodes and solves the finite element problem repeatedly to determine the lumped capacitances. Since the electronics of the commercial sensor detect displacements by monitoring only changes in the capacitance between the sensing electrode and target, the lumped capacitance identified as C_{14} is of primary interest.

3.2 Capacitance as a Function of Gap and Target Diameter. The apparent sensitivity for a particular target diameter is obtained by repeatedly applying the finite element procedure to calculate the lumped capacitance C_{14} between the sensing electrode and target as a function of the gap. The capacitance is calculated for spherical targets with diameters of 6.35, 9.53, 12.70, 15.88, 19.05, 22.23, and 25.40 mm. For comparison, the lumped capacitance is also calculated as a function of the gap for a flat target. The lumped capacitance is calculated with gap increments of 5.1 μm for the low sensitivity and 1.016 μm for the high sensitivity. Twelve or fifteen increments of the gap are analyzed for each spherical diameter. Capacitance values are not calculated for a spherical diameter of 6.35 mm and the high sensitivity since the required sensing range was unreasonably close to the target. A listing of the computed values for C_{14} is available from Smith [41]. The values of capacitance for the low sensitivity range between 0.217 and 0.526 pF. The capacitances for the high sensitivity range between 0.593 and 1.822 pF.

4 Effects of Spherical Targets

The computed values for the lumped capacitance between the sensing electrode and target C_{14} reveal four effects of spherical targets. As the diameter of the target is reduced, the sensing range decreases and the sensing range shifts toward the target. Furthermore, the apparent sensitivity and nonlinearity increase, which is more important to the accuracy of measurements. All of these effects become more pronounced when sensors have high sensitivity and the diameter of the target is small.

4.1 Shift of Nominal Gap and Reduction of Sensing Range. Figures 7 and 8 show plots of the inverse of the lumped capacitance between the sensing electrode and target ($1/C_{14}$) as a function of the gap distance and the diameter of the target. For an ideal sensor, each curve should be a straight line with positive slope; recall that the sensitivities are defined as negative values, which changes the sign of the slope. Vertical lines show the minimum, nominal, and maximum gaps for a flat target (from Table 1);

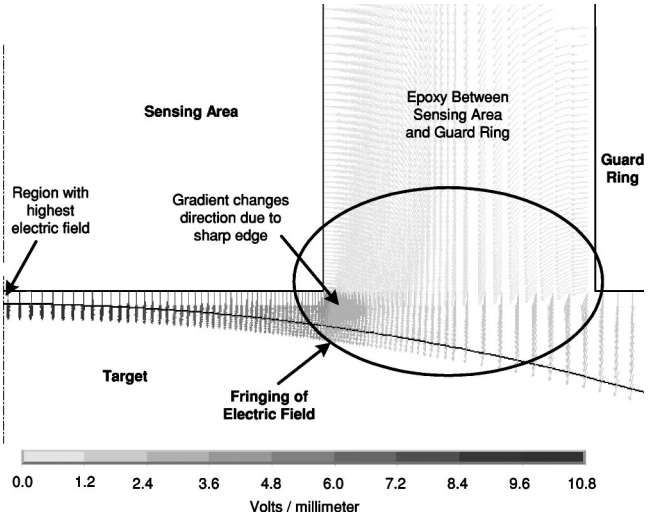

Fig. 5 Electric field in vicinity of sensing electrode

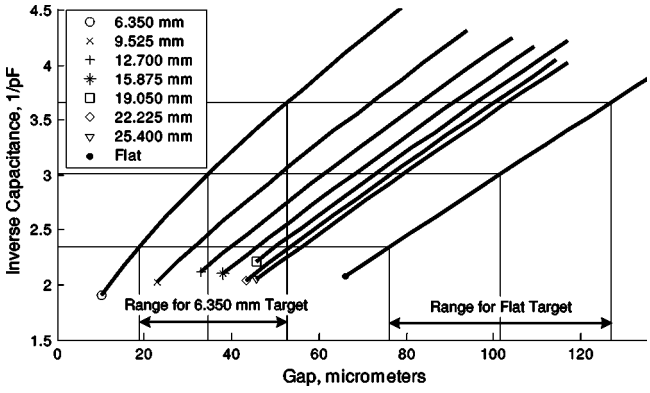

Fig. 7 Inverse capacitance for low sensitivity (-0.394 V/μm) as a function of the gap and target diameter

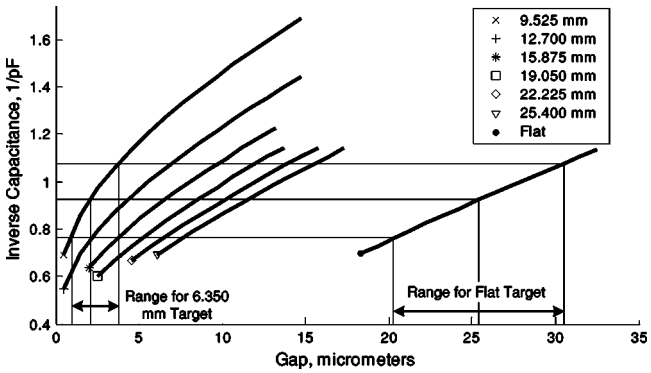

Fig. 8 Inverse capacitance for high sensitivity (-1.694 V/μm) as a function of the gap and target diameter

reflecting these lines onto the ordinate gives the inverse capacitances that correspond to the minimum, nominal, and maximum gaps for a flat target.

The minimum, nominal, and maximum gaps for each spherical target is estimated by finding the intersection of the horizontal lines and each inverse capacitance curve. This method is illustrated for the ∅6.35 mm target at low sensitivity in Fig. 7 and for the ∅9.53 mm target at high sensitivity in Fig. 8. For the low sensitivity, the nominal gap shifts from about 102 μm for a flat target to about 35 μm for a ∅6.35 mm target, and the range is reduced from about 51 μm to about 34 μm. For high sensitivity, the nominal gap shifts from about 25 μm for a flat target to about 2 μm for a ∅9.53 mm target, and the range shifts from about 10 μm to a mere 2.8 μm. The shift and reduction in sensing ranges for the remaining targets and sensitivities are tabulated in Tables 2 and 3. These results demonstrate the significant error associated with using commercial sensors (calibrated on flat surfaces) with spherical targets.

4.2 Increase in Sensitivity and Nonlinearity. The inverse capacitance of the previous section must be related to output voltage in order to evaluate changes in the sensitivity and nonlinearity of the output. The sensing law given in Eq. (3) indicates that the voltage V output by the sensing system is linearly proportional to changes in the gap Δg. As shown in Eq. (5), a change in the gap should be measured with respect to the nominal gaps for different spherical targets that were listed in Tables 2 and 3

$$\Delta g = g - g_{\text{nom}} \tag{5}$$

The electronics of the sensor produce a ± 10 V signal as the inverse capacitance varies between the minimum and maximum values for flat targets. At low sensitivity, the inverse capacitance ranges between 2.347 and 3.663 pF^{-1}; at high sensitivity, the inverse capacitance ranges between 0.763 and 1.078 pF^{-1}. The electronic gain G is estimated from these values with Eq. (6). The gains are determined to be $G=-15.2$ V-pF and $G=-63.5$ V-pF for the low and high sensitivities, respectively,

$$G = -\frac{V_{\max} - V_{\min}}{\left(\frac{1}{C_{14}}\right)_{\max} - \left(\frac{1}{C_{14}}\right)_{\min}} \tag{6}$$

Equation (7) shows that the inverse capacitance curves are related to voltage by multiplying the gain of the electronics with the difference between the inverse capacitance $1/C_{14}$ and nominal inverse capacitance $(1/C_{14})_{\text{nom}}$. The nominal inverse capacitances for the low and high sensitivities were 0.332 and 1.083 pF^{-1}, respectively, as shown in Figs. 7 and 8,

$$V = G\left[\frac{1}{C_{14}} - \left(\frac{1}{C_{14}}\right)_{\text{nom}}\right] \tag{7}$$

Plots of the expected voltage output, as a function of changes in the gap, can be determined for each spherical diameter by computing Δg with Eq. (5) and V with Eq. (7). Figures 9 and 10 show the voltages as a function of the change in gap for the low and high sensitivities. It is clear from these plots that the slope, which equals the sensitivity S, increases as the diameter of the target

Table 2 Predicted changes in the gap and sensing range for low sensitivity (-0.394 V/μm)

Diameter (mm)	Gap			Change in nominal gap (%)	Sensing range (μm)	Change in range (%)
	Min gap (μm)	Nom gap (μm)	Max gap (μm)			
6.35	18.8	34.7	52.8	−66	34.0	−33
9.53	31.5	51.0	72.0	−50	40.5	−20
12.70	40.0	61.2	83.4	−40	43.4	−15
15.88	45.8	68.0	91.0	−33	45.2	−11
19.05	50.1	72.9	96.3	−28	46.2	−9
22.23	53.3	76.5	100.2	−25	46.9	−8
25.40	55.8	79.4	103.3	−22	47.5	−6
Flat	76.2	101.6	127.0	0	50.8	0

Table 3 Predicted changes in the gap and sensing range for high sensitivity (-1.969 V/μm)

Diameter (mm)	Gap			Change in nominal gap (%)	Sensing range (μm)	Change in range (%)
	Min gap (μm)	Nom gap (μm)	Max gap (μm)			
6.35	—	—	—	—	—	—
9.53	1.0	2.1	3.8	−92	2.8	−73
12.70	2.2	4.3	7.0	−83	4.8	−53
15.88	3.7	6.5	9.7	−74	6.0	−41
19.05	5.2	8.5	12.1	−67	6.9	−32
22.23	6.5	10.1	14.0	−60	7.5	−26
25.40	7.6	11.5	15.6	−55	8.0	−22
Flat	20.3	25.4	30.5	0	10.2	0

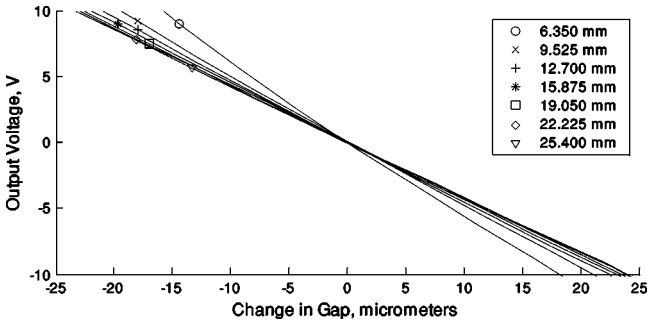

Fig. 9 Voltage as a function of the change in gap for each spherical target and low sensitivity (predicted by FEA)

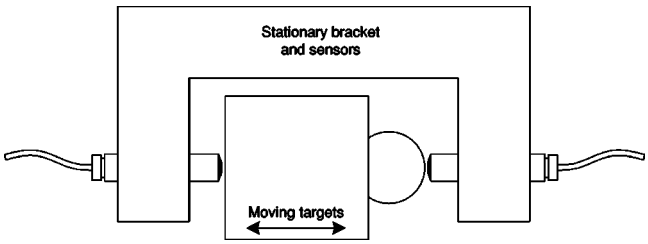

Fig. 11 Fixture used to compare the output of sensors targeting spherical and flat surfaces. The sensors are stationary while the target surfaces move using the cross axis of the measuring machine.

decreases. Furthermore, the nonlinearity increases as the diameter of the target decreases. This effect is most pronounced for the high sensitivity.

Apparent sensitivities, listed in Table 4, are computed by finding the slope of the least-squares lines through the data points that lie within the ± 10 V range. As the diameter of the spherical target increases, the sensitivities asymptotically approach that of a flat target (-0.394 and -1.969 V/μm). For the $\varnothing$6.35 mm target and low sensitivity, the percent change in sensitivity is 48%. For the $\varnothing$9.53 mm target and high sensitivity, the percent change in sensitivity is 147%. The 25.4 mm target has significantly smaller changes in sensitivity, however.

5 Experimental Validation

The finite element models described in the previous section can be experimentally validated using capacitive sensor systems and targets of varying diameter. The experimental hardware used for this validation allows comparison of the output from two capacitive sensors while minimizing the influence of off-axis motion and thermal gradients through thoughtful design.

Figure 11 shows the hardware used to validate the finite element models. The two sensors are held in the same bracket so that any relative motion between one sensor and its target is equal and opposite to the relative motion between the second sensor and its target. The testing is performed on a precision Moore No. 3 Universal Measuring Machine with collinear sensors in accordance with the Abbe Principle to minimize the effects of any off-axis motions. The sensor bodies are aligned to within 20 arc-seconds of the axes of travel. During testing, the machine table is moved in the direction along the sensor axes.

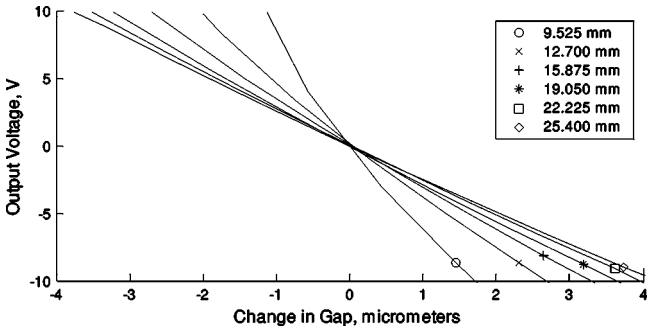

Fig. 10 Voltage as a function of the change in gap for each spherical target and high sensitivity (predicted by FEA)

The first (left-hand) sensor always targets a precision-ground flat reference surface while the second (right-hand) sensor targets either a flat surface for calibration or spheres of varying diameter. During calibration with two flat target surfaces the sensor output repeats within 20 nm and matches the manufacturer's calibration data within 0.25%, which is negligibly small compared to the effects observed due to target diameter. This result confirms the accuracy of the sensor alignment, and the insensitivity of the experimental hardware to vibration, noise, and thermal drift.

Prior to testing, the importance of sensor centering and perpendicularity to the spherical target was explored experimentally. In practice, this is equivalent to finding the ''high spot'' on the target sphere. This geometric effect is not included in the axisymmetric finite element model and is difficult to completely eliminate in the actual hardware. By checking the repeatability of the comparative sensor output with different amounts of deliberate decentering, it was found that the effect is negligible for sensor centering within 50 μm of the high spot. It is straightforward to find the high spot to within 25 μm or better using the three axes of the Moore measuring machine, thereby satisfying this requirement. Once the highest point on each sphere is found, both capacitive sensors are adjusted axially in the sensor bracket such that each sensor is within one micrometer of the middle of its sensing range (nominally zero Volts from the sensors' electronic output).

During each test, the machine is slowly actuated while both sensors measure several full cycles of motion over the sensing range. When the two sensors target flat surfaces, the output is linear over the range of travel. However, the relationship becomes nonlinear when a spherical target replaces the second reference flat. As predicted by the finite element results, the comparative sensor output shows a nominally linear relationship with addi-

Table 4 Comparison of apparent sensitivities determined experimentally and by finite element analyses

	Nominal sensitivity: 0.394 V/μm			Nominal sensitivity: 1.969 V/μm		
Target (mm)	FEA (V/μm)	Exp. (V/μm)	Difference (%)	FEA (V/μm)	Exp. (V/μm)	Difference (%)
Flat	0.394	0.394	0.0	1.969	1.967	0.1
25.40	0.422	0.419	0.7	2.501	2.448	2.1
22.23	0.426	0.425	0.2	2.662	2.591	2.7
19.05	0.432	0.430	0.5	2.882	2.762	4.2
15.88	0.442	0.438	0.9	3.310	3.528	−6.6
12.70	0.455	0.455	0.0	4.103	4.434	−8.1
9.53	0.487	0.489	−0.4	6.167	N/A	N/A
6.35	0.583	0.572	1.9	N/A	N/A	N/A

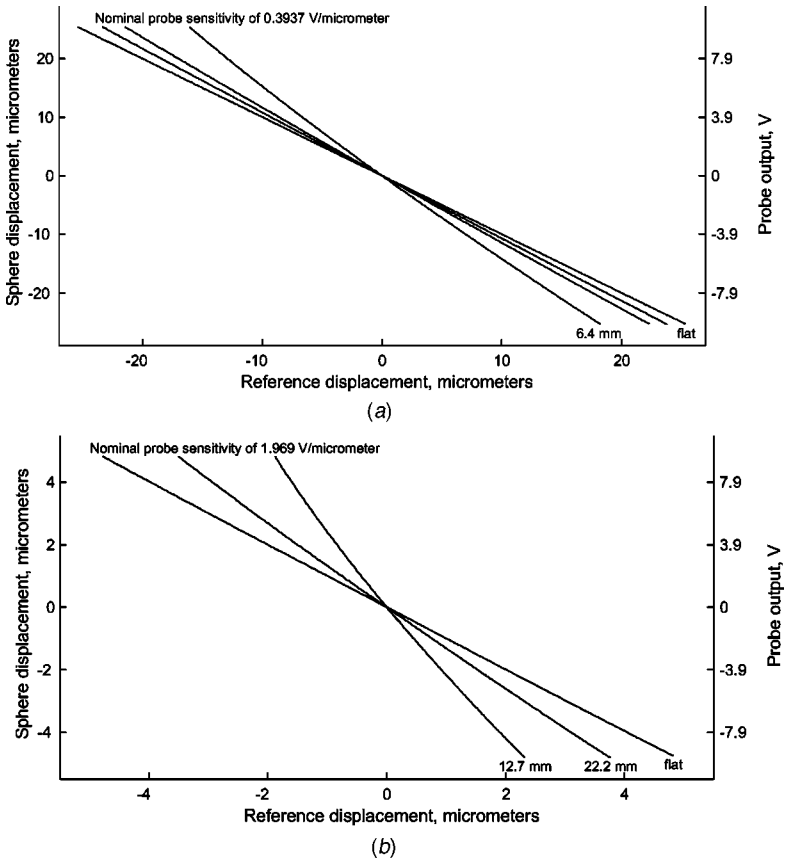

Fig. 12 Comparison of experimental sensor output for different target diamenters (*a*) for −0.3937 V/μm and (*b*) for −1.969 V/μm

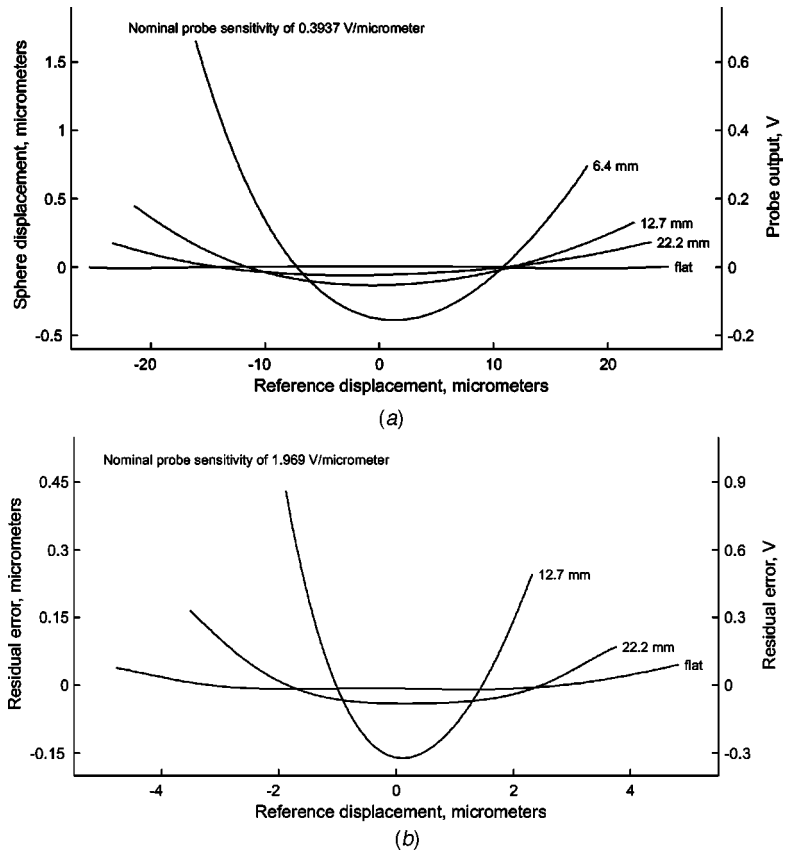

Fig. 13 Residual nonlinearity in experimental sensor output (*a*) −0.3937 V/μm and (*b*) for −1.969 V/μm

tional higher-order behavior. The data show both the apparent sensitivity of the spherical target (the linear portion) and the nonlinear residual. The results tabulated in Table 4 show excellent agreement with the finite element models. The maximum discrepancy between model and experiment was less than 2% for the $-0.394\ \mathrm{V}/\mu\mathrm{m}$ sensor system less than about 8% for the $-1.969\ \mathrm{V}/\mu\mathrm{m}$ sensitivity.

Figures 12(*a*) and 12(*b*) show the relationship between the outputs from the two sensors for both nominal sensitivities (-0.394 and $-1.969\ \mathrm{V}/\mu\mathrm{m}$). The abscissa is the output of the sensor targeting the flat reference surface, and the ordinate is the output of the sensor targeting the sphere. These plots show that the relationship deviates increasingly from the ideal straight line of slope$=-1$ as the target diameter decreases. Figures 13(*a*) and 13(*b*) show the residual after the best fit linear function is removed. Ideally, the two flat targets should be perfectly linear and the residual should be zero. The experimental measurements with flat targets show residuals consistent with the manufacturer's calibration data sheet. When the target diameter is increasingly small, the residual portion becomes significant and the figures provide representative estimates for the accuracy of a modern capacitive sensor system.

6 Conclusion

Capacitive displacement sensors for precision manufacturing and metrology are often used with spherical targets despite being calibrated with flat surfaces at the factory. This paper elucidates four effects of this standard practice. First, the sensitivity of the sensing system increases, which tends to exaggerate actual displacements. Second, increases in the sensitivity reduce the size of the sensing range. Third, as the diameter of the target electrode decreases, the sensing range shifts closer to the target electrode. Fourth and perhaps most important when striving for accurate measurements, the relation between the output voltage and displacement becomes increasingly nonlinear as the diameter of the spherical target decreases.

The finite element analysis and the experimental approach described in this paper prove to be equally valid techniques for quantifying these effects in a particular capacitive displacement-sensing system. For a representative sensor, these approaches indicate that the error in sensitivity may be as much as 150% and that the nonlinearity may prevent accurate measurements with small diameter targets. Furthermore, the sensing range can shift so near the target that it becomes essentially impossible to even make measurements.

Since these effects lead to measurement error, precision manufacturing and metrology applications requiring the highest accuracy should correct the output of the sensor or use sensors factory calibrated with a particular spherical target. For all but the smallest targets, sufficiently accurate measurements are obtainable with corrected sensitivities. For the smallest spheres where nonlinearities are significant, a higher-order correction is likely necessary. Alternatively, using a sensor with a smaller sensing area can reduce the error, and this aspect can be investigated in future work.

References

[1] ANSI/ASME B5.54, 1992, *Methods for Performance Evaluation of Computer Numerically Controlled Machining Centers*, ASME, New York.

[2] ANSI/ASME B5.57, 2000, *Methods for Performance Evaluation of Computer Numerically Controlled Lathes and Turning Centers*, ASME, New York.

[3] ANSI/ASME B89.3.4M, 1985, *Axes of Rotation–Methods for Specifying and Testing*, ASME, New York.

[4] Grejda, R. D., 2002, "Use and Calibration of Ultra Precision Axes of Rotation with Nanometer Level of Metrology," Ph.D. thesis, Penn State University, State College, PA.

[5] Morgan, V. T., and Brown, D. E., 1969, "A Differential-Capacitance Transducer for Measuring Small Displacements," J. Phys. E, **2**, pp. 793–795.

[6] Jones, R. V., and Richards, J. C. S., 1973, "The Design and Some Applications of Sensitive Capacitance Micrometers," J. Phys. E, **6**, pp. 589–600.

[7] Stacey, F. D., Rynn, J. M. W., Little, E. C., and Croskell, C., 1969, "Displacement and Tilt Transducers of 140 dB Range," J. Phys. E, **2**, pp. 945–949.

[8] Schofield, J. W., 1972, "A Linear Capacitance Micrometer," J. Phys. E, **5**, pp. 822–825.

[9] Sydenham, P. H., 1972, "Microdisplacement Transducers," J. Phys. E, **5**, pp. 721–733.

[10] Rigden, J. D., 1977, "A Capacitive Bore Gauge," J. Phys. E, **10**, pp. 1276–1278.

[11] Hicks, T. R., Reay,, N. K. and Atherton, P. D., 1984, "The Application of Capacitance Micrometry to the Control of Fabry-Perot Etalons," J. Phys. E, **17**, pp. 49–55.

[12] Wolfendale, P. C. F., 1968, "Capacitive Displacement Transducers with High Accuracy and Resolution," J. Phys. E, **2**, pp. 817–818.

[13] de Jong, G. W., and Meijer, G. C. M., 1997, "An Efficient Retrieving Algorithm for Accurate Capacitive Position Sensors," Sens. Actuators, A, **58**, pp. 75–84.

[14] Kolb, P. W., Decca,, R. S. and Drew, H. D., 1988, "Capacitive Sensor for Micropositioning in Two Dimensions," Rev. Sci. Instrum., **69**(1), pp. 310–312.

[15] Hague, B., and Foord, T. R., 1971, *Alternating Current Bridge Methods*, Pittman, London.

[16] Hugill, A. L., 1982, "Displacement Transducers Based on Reactive Sensors in Transformer Ratio Bridges," J. Phys. E, **15**, pp. 597–606.

[17] Dratler, J., 1977, "Inexpensive Linear Displacement Transducer Using a Low Power Lock-In Amplifier," Rev. Sci. Instrum., **48**(3), pp. 327–335.

[18] Huang, S. M., Stott, A. L., Green, R. G., and Beck, M. S., 1988, "Electronic Transducers for Industrial Measurement of Low Value Capacitances," J. Phys. E, **21**, pp. 242–250.

[19] Ashrafi, A., and Golnabi, H., 1999, "A High Precision Method for Measuring Very Small Capacitance Changes," Rev. Sci. Instrum., **70**(8), pp. 3483–3487.

[20] Lányi, S., and Hrukovic, M., 2001, "Linearization of Inverse-Capacitance-Based Displacement Transducers," Meas. Sci. Technol., **12**, pp. 77–81.

[21] Fritsch, K., 1987, "Linear Capacitive Displacement Sensor With Frequency Readout," Rev. Sci. Instrum., **58**(5), pp. 861–863.

[22] Richards, J. C. S., 1976, "Linear Capacitance Proximity Gauges with High Resolution," J. Phys. E, **9**, 639–646.

[23] Maxwell, J. C., 1873, *A Treatise on Electricity and Magnetism*, Vol. 1, Oxford Univ. Press, New York.

[24] Heerens, W. C., and Vermeulen, F. C., 1975, "Capacitance of Kelvin Guard-Ring Capacitors with Modified Edge Geometry," J. Appl. Phys., **46**, pp. 2486–2490.

[25] Heerens, W. C., 1976, "The Solution of Laplace's Equation in Cylindrical and Toroidal Configurations with Rectangular Sectional Shapes and Rotation-Symmetrical Boundary Conditions," J. Appl. Phys., **47**(8), pp. 3740–3744.

[26] Heerens, W. C., 1986, "Application of Capacitance Techniques in Sensor Design," J. Phys. E, **19**, pp. 897–906.

[27] Lazzarini, A., 1986, "Sources of Error in Dynamic Applications of Electronic Displacement Sensors," Rev. Sci. Instrum., **57**(12), pp. 3099–3106.

[28] Hicks, T., and Atherton, P. D., 2000, *Nanopositioning Book*, Penton Press, London.

[29] Rosa, E. B., and Dorsey, N. E., 1907, Bull. Bur. Stds., **3**, pp. 433–604.

[30] Khan, A. R., Brown, I. J., and Brown, M. A., 1980, "The Behavior of Capacitance Displacement Transducers Using Epoxy Resin as an Electrode-Guard Ring Spacer," J. Phys. E, **13**, pp. 1280–1281.

[31] Genossar, J., and Steinitz, M., 1990, "A Tilted-Plate Capacitance Displacement Sensor," Rev. Sci. Instrum., **61**(9), pp. 2469–2471.

[32] Harb, S. M., Chetwynd, D. G., and Smith, S. T., 1995, "Tilt Errors in Parallel Plate Capacitive Micrometry," *International Progress in Precision Engineering 8th International Precision Engineering Seminar*, Elsevier, Compiegne, France pp. 147–150.

[33] Brown, M. A., and Bulleid,, C. E., 1978, "The Effect of Tilt and Surface Damage on Practical Capacitance Displacement Transducers," J. Phys. E, **11**, pp. 429–432.

[34] Puers, R., and Lapadatu, D., 1996, "Electrostatic Forces and Their Effects on Capacitive Mechanical Sensors," Sens. Actuators, A, **56**, pp. 203–210.

[35] Bonse, M. H. W., Mul, C., and Spronck, J. W., 1995, "Finite-Element Modelling as a Tool for Designing Capacitive Position Sensor," Sens. Actuators, A, **46-47**, pp. 266–269.

[36] Ansel, Y., Romanowicz, B., Renaud,, P. and Schrofer, G., 1998, "Global Model Generation for a Capacitive Silicon Accelerometer by Finite Element Analysis," Sens. Actuators, A, **67**, pp. 153–158.

[37] Khan, S. H., Grattan, K. T. V., and Finkelstein, L., 1999, "Investigation of Leakage Flux in a Capacitive Angular Displacement Sensor Used in Torque Motors by 3D Finite Element Field Modeling," Sens. Actuators, A, **76**, pp. 253–259.

[38] Kuijpers, A. A., Krijnen, G. J. M., Wiegerink, R. J., Lammerink, T. S. J., and Elwenspoek, M., 2003, "2D-Finite-Element Simulations for Long-Range Capacitive Position Sensor," J. Micromech. Microeng., **13**, pp. S183–S189.

[39] Lányi, S., 1998, "Analysis of Linearity Errors of Inverse Capacitance Position Sensors," Meas. Sci. Technol., **9**, pp. 1757–1764.

[40] Gladwin, M. T., and Wolfe, J., 1975, "Linearity of Capacitance Displacement Transducers," Rev. Sci. Instrum., **46**(8), pp. 1099–1100.

[41] Smith, P., 2003, *Analysis and Application of Capacitive Displacement Sensors to Curved Surfaces*, Master's thesis, University of Kentucky, Lexington, KY.